2D Scattering Analysis through Meshless Methods: A Comparison Between Two Different Shape Function Schemes

Williams L. Nicomedes, Renato C. Mesquita* and Fernando J. S. Moreira
Dept. of Electronics Engineering and *Dept. of Electrical Engineering
Federal University of Minas Gerais (UFMG), Belo Horizonte, Brazil
wlnicomedes@yahoo.com.br; renato@ufmg.br; fernandomoreira@ufmg.br

***Abstract*—In this paper we apply a meshless method to the classical electromagnetic scattering integral field equations. These equations are discretized via two different schemes related to the construction of shape functions: the Moving Least Squares (MLS) and the Improved Moving Least Squares (IMLS) approximations. We then establish a comparison between these two approximations in what concerns to their applicability and rates of convergence.**

Keywords- Meshless; MLS; IMLS; scattering; integral equations

I. INTRODUCTION

When solving scattering problems through integral formulations, the widespread Method of Moments (MoM) is generally employed [1]. In MoM, depending on the choices for the basis and testing functions, different results come out, being the rectangular unit pulse or the triangular pulse (as basis) and the Dirac delta (as testing) of most common usage. In the present work we discretize the classical integral equations through a different kind of basis functions: the shape functions that arise in meshless methods. Meshless methods have been applied as an alternative to the Finite Element Method (FEM) because, as one of its advantages, it requires no mesh generation [2],[3],[4]. These shape functions don't have analytical expressions, being built numerically during the solution of the problem, and there are a number of different ways to build them. We have then chosen two among these ways: the MLS and the IMLS approaches, and applied them to the scattering integral equations, seeking for the one that is most suitable.

II. THE MESHLESS APPROACH

A. Presentation

The meshless approach begins by spreading nodes over the domain of the problem to be solved. Nodes are simple points and to each one a shape function is associated. Each shape function has the property of being zero over the whole domain, except in the vicinity of the corresponding node. The vicinal region in which the shape function is different from zero is the node's *influence domain* [5]. The main difference between meshless methods and mesh-based methods (like the FEM) is that the *element* concept is not present. The influence domains are arbitrary (the only restriction is that the set of influence domains must cover the entire domain) and can overlap. So, the nodes can be distributed arbitrarily without generating an element mesh.

For a given point (e.g. point $\vec{x} = X$ in Fig. 1), an unknown solution u is expressed as a sum of the contributions of those nodes that influence X, i.e. nodes that extend their influence domains onto X (they are depicted inside the circular shaded region):

$$u(\vec{x}) \sim u^h(\vec{x}) = \sum_{i=1}^{N} \phi_i(\vec{x})\hat{u}_i = \boldsymbol{\Phi}(\vec{x})\boldsymbol{u} \qquad (1)$$

where u^h is the approximated solution, N is the number of nodes whose influence domains include the point $\vec{x}$, each ϕ_i is the i-th node shape function evaluated at $\vec{x}$, and $\hat{u}_i$ is the associated nodal parameter.

B. Shape Function Construction

The methods we have employed to build the shape functions are the MLS and IMLS.

1) The MLS Approach

In the MLS, u^h is expressed as:

$$u^h(\vec{x}) = \sum_{j=1}^{m} p_j(\vec{x})a_j(\vec{x}) = \boldsymbol{p}^T(\vec{x})\boldsymbol{a}(\vec{x}) \qquad (2)$$

where $\boldsymbol{p}$ is a monomial basis with m terms (e.g. $\boldsymbol{p}(\vec{x}) = [1, x, y]$) and $\boldsymbol{a}$ is a vector of coefficients which are functions of $\vec{x}$. We then build a slightly different approximation, by requiring the monomial basis to be calculated at each node:

$$u^h(x, \vec{x}_i) = \sum_{j=1}^{m} p_j(\vec{x}_i)a_j(\vec{x}) = \boldsymbol{p}^T(\vec{x}_i)\boldsymbol{a}(\vec{x}) \qquad (3)$$

The next step is to define a weighted functional M:

$$M = \sum_{i=1}^{N} w\left(\frac{\|\vec{x} - \vec{x}_i\|}{d_i}\right)[u^h(\vec{x}, \vec{x}_i) - \hat{u}_i]^2 \qquad (4)$$

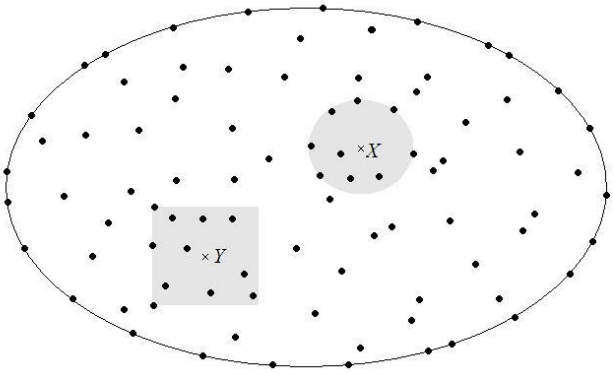

Figure 1. Nodes spread in a domain. Those ones that influence points X and Y are shown as belonging to regions that surround these points (shaded regions).

or

$$M = \sum_{i=1}^{N} w\left(\frac{\|\vec{x} - \vec{x}_i\|}{d_i}\right)\left[\sum_{j=1}^{m} p_j(\vec{x}_i)a_j(\vec{x}) - \hat{u}_i\right]^2 \quad (5)$$

where d_i is the size of the influence domain associated to node i and w is a function with compact support centered in node i. We have chosen it to be a cubic spline [5]:

$$w = \begin{cases} 2/3 - 4r^2 + 4r^3 & ,0 \le r \le 0.5 \\ 4/3 - 4r + 4r^2 - 4/3\, r^3 & ,0.5 < r \le 1 \\ 0 & ,r > 1 \end{cases} \quad (6)$$

where $r = \|\vec{x} - \vec{x}_i\|/d_i$. Looking for the coefficients a_j that minimize the functional, we have imposed

$$\frac{\partial M}{\partial \boldsymbol{a}} = 0 \quad (7)$$

After some matrix manipulation, we obtain

$$\boldsymbol{a}(\vec{x}) = [\boldsymbol{A}(\vec{x})]^{-1}[\boldsymbol{B}(\vec{x})]\boldsymbol{u} \quad (8)$$

where

$$\boldsymbol{u}^T = [\hat{u}_1, \hat{u}_2, \ldots, \hat{u}_N] \quad (9)$$

$$\boldsymbol{A}(\vec{x}) = \boldsymbol{P}^T\boldsymbol{W}(\vec{x})\boldsymbol{P} \quad (10)$$

$$\boldsymbol{B}(\vec{x}) = \boldsymbol{P}^T\boldsymbol{W}(\vec{x}) \quad (11)$$

which are given in terms of

$$\boldsymbol{P} = \begin{bmatrix} p_1(\vec{x}_1) & \cdots & p_m(\vec{x}_1) \\ \vdots & \ddots & \vdots \\ p_1(\vec{x}_N) & \cdots & p_m(\vec{x}_N) \end{bmatrix} \quad (12)$$

$$\boldsymbol{W}(\vec{x}) = \begin{bmatrix} w\left(\frac{\|\vec{x} - \vec{x}_1\|}{d_1}\right) & \cdots & 0 \\ \vdots & \ddots & \vdots \\ 0 & \cdots & w\left(\frac{\|\vec{x} - \vec{x}_N\|}{d_N}\right) \end{bmatrix} \quad (13)$$

By equating the expressions (1) and (2) the shape functions are readily available:

$$\boldsymbol{\Phi}(\vec{x}) = [\phi_1(\vec{x}), \ldots, \phi_N(\vec{x})] = \boldsymbol{p}^T\boldsymbol{A}^{-1}(\vec{x})\boldsymbol{B}(\vec{x}) \quad (14)$$

2) *The IMLS Approach*

The MLS approximation doesn't always provide useful shape functions, because sometimes the A-matrices become singular, preventing inversion. This phenomenon occurs for some scatterer geometries, like the rectangular one. To avoid the problem of getting singular matrices a somewhat different approach, known as IMLS was developed [6].

In the IMLS, it is required that the terms of the basis $\boldsymbol{p}$ be orthogonal to each other, *only at the nodal points*. In order to do so, they are viewed as belonging to a Hilbert space in which the following inner product between functions f and g is defined:

$$\langle f, g\rangle = \sum_{I=1}^{N} w(\vec{x} - \vec{x}_I)f(\vec{x}_I)g(\vec{x}_I) \quad (15)$$

where w is the function defined in (6). The orthogonality condition is assured through the property $(k, j = 1,2, \ldots, m)$:

$$\langle p_k, p_j\rangle = \sum_{I=1}^{N} w(\vec{x} - \vec{x}_I)p_k(\vec{x}_I)p_j(\vec{x}_I) = \begin{cases} A_k, k = j \\ 0, k \ne j \end{cases} \quad (16)$$

As already said, the terms $p_1 \ldots p_m$ of the basis $\boldsymbol{p}$ are orthogonal only about the nodal points. Given a general point $\vec{x}$, one finds out the N nodes that influence it and evaluates the expression in (16).

Bearing in mind the orthogonality at the nodal points, one forms the basis $\boldsymbol{p}$ by requiring its first term to be equal to the unity everywhere, i.e.

$$p_1(\vec{x}) = 1 \quad (17)$$

the next terms are formed recursively:

$$p_i = r^{i-1} - \sum_{k=1}^{i-1} \frac{\langle r^{i-1}, p_k\rangle}{\langle p_k, p_k\rangle} p_k, \quad i = 2,3, \ldots m \quad (18)$$

where r is the radial distance from the given point $\vec{x}$.

Taking the linear system expressed by (8),

$$\boldsymbol{A}(\vec{x})\boldsymbol{a}(\vec{x}) = \boldsymbol{B}(\vec{x})\boldsymbol{u} \quad (19)$$

substituting the expressions for $\boldsymbol{A}$ and $\boldsymbol{B}$ (10,11,12,13) and recalling the orthogonality conditions (16), the following linear system is obtained:

$$\begin{bmatrix} \langle p_1, p_1 \rangle & \cdots & 0 \\ \vdots & \ddots & \vdots \\ 0 & \cdots & \langle p_m, p_m \rangle \end{bmatrix} \begin{bmatrix} a_1(\vec{x}) \\ \vdots \\ a_m(\vec{x}) \end{bmatrix} = \begin{bmatrix} \langle p_1, \boldsymbol{u} \rangle \\ \vdots \\ \langle p_m, \boldsymbol{u} \rangle \end{bmatrix}$$

which, when solved, gives:

$$\begin{bmatrix} a_1(\vec{x}) \\ \vdots \\ a_m(\vec{x}) \end{bmatrix} = \begin{bmatrix} \frac{1}{\langle p_1, p_1 \rangle} & \cdots & 0 \\ \vdots & \ddots & \vdots \\ 0 & \cdots & \frac{1}{\langle p_m, p_m \rangle} \end{bmatrix} \begin{bmatrix} \langle p_1, \boldsymbol{u} \rangle \\ \vdots \\ \langle p_m, \boldsymbol{u} \rangle \end{bmatrix} \quad (20)$$

Calling this new matrix $\overline{\boldsymbol{A}}(\vec{x})$ and as $(\langle p_1, \boldsymbol{u} \rangle, \ldots, \langle p_m, \boldsymbol{u} \rangle) = \boldsymbol{B}(\vec{x})\boldsymbol{u}$, we have for the coefficients $\boldsymbol{a}$:

$$\boldsymbol{a}(\vec{x}) = \overline{\boldsymbol{A}}(\vec{x})\boldsymbol{B}(\vec{x})\boldsymbol{u} \quad (21)$$

which is an expression analogous to (8), but requires no matrix inversion. Once the inner products are always positive and different from zero, $\overline{\boldsymbol{A}}$ is always nonsingular, thus providing correct values for the coefficients $\boldsymbol{a}$. (21) is then substituted back in (2), and a comparison with (1) makes explicit the expression for the shape functions:

$$\boldsymbol{\Phi}(\vec{x}) = [\phi_1(\vec{x}), \ldots, \phi_N(\vec{x})] = \boldsymbol{p}^T(\vec{x})\overline{\boldsymbol{A}}(\vec{x})\boldsymbol{B}(\vec{x}) \quad (22)$$

III. SCATTERING ANALYSIS

A. Integral Equations

The problem to be analyzed is that of a normally incident monochromatic TM^z plane wave scattered by an infinite perfectly electric conductor (PEC) cylinder. The scattered field can be evaluated after the induced surface electric current density J_s is determined. For a cylinder infinite in the z-direction, along which the current flows ($J_s \to J_z$), no quantity is dependent upon z. Hence, the problem is two-dimensional and the calculations are made only regarding the cylinder cross-section. The incident TM plane wave, coming from the left and having only the z-component is:

$$E_z^i(\vec{x}) = E_z^i(x, y) = E_0 e^{-jkx} \quad (23)$$

where E_0 is an amplitude constant and $k = 2\pi/\lambda$ is the wavenumber (λ being the wavelength).

Two integral equations are cast for the numerical solution of the scattering problem. By reasoning about the electric field, from the boundary condition for the total field (incident and scattered)

$$E_z^i(\vec{x}) + E_z^s(\vec{x}) = 0 \; at \; the \; cylinder \; surface \quad (24)$$

and from the expression for the scattered field [1]

$$E_z^s(\vec{x}) = \left(\frac{\nabla\nabla\cdot + k^2}{j\omega\varepsilon}\right) \oint J_z(\vec{x}') H_0^{(2)}(kR) dl' \quad (25)$$

one obtains the Electric Field Integral Equation (EFIE):

$$E_z^i(\vec{x}) = \frac{\omega\mu}{4} \oint J_z(\vec{x}') H_0^{(2)}(kR) dl' \quad (26)$$

where $\vec{x}$ and $\vec{x}'$ locate the observation and source points at the cylinder cross-section perimeter, respectively, $R = \|\vec{x} - \vec{x}'\|$, $\omega = 2\pi f$, where f is the wave frequency, ε is the permittivity of the medium, and $H_0^{(2)}$ is the zero-order Hankel function of the second type. The integral (18) is to be evaluated over the entire perimeter of the cross-section.

By reasoning about the magnetic field, from the boundary condition (also at the cylinder surface)

$$\hat{\boldsymbol{n}} \times \left[\vec{H}^i(\vec{x}) + \vec{H}^s(\vec{x})\right] = \vec{J}_s(\vec{x}) = \hat{\boldsymbol{z}} J_z(\vec{x}) \quad (27)$$

and from the expression for the scattered field [1]

$$\vec{H}^s(\vec{x}) = \nabla \times \hat{\boldsymbol{z}} \oint J_z(\vec{x}') H_0^{(2)}(kR) dl' \quad (28)$$

the Magnetic Field Integral Equation (MFIE) is obtained:

$$\hat{\boldsymbol{n}} \times \vec{H}^i(\vec{x}) = \hat{\boldsymbol{z}} J_z(\vec{x}) - \hat{\boldsymbol{n}} \times \nabla \times \hat{\boldsymbol{z}} \oint J_z(\vec{x}') H_0^{(2)}(kR) dl' \quad (29)$$

In principle, both EFIE and MFIE can be used to solve for J_z. However, spurious resonant solutions may come into the scene and compromise the precision of the numerical evaluation, especially for an electrically large cylinder cross-section [1]. The resonance problem can be avoided by a linear combination of (26) and (29):

$$CFIE = \alpha \; EFIE + (1 - \alpha)\, \eta \; MFIE \quad (30)$$

where α is a parameter ranging from zero to one and η is the intrinsic impedance of the exterior medium. Equation (30) is the Combined Field Integral Equation (CFIE) and α is generally set equal to 0.5 [1].

B. CFIE Meshless Numerical Solution

The problem at hand consists of numerically evaluating the surface integral equation (30) in order to obtain the surface electric current J_z. Nodes are then spread along the perimeter of the cylinder cross section (Fig. 2). Expressing the surface current as a sum of shape functions built through the MLS approximation there follows:

$$J_z(\vec{x}) = \sum_{i=1}^{N} \phi_i(\vec{x}) \hat{u}_i \quad (31)$$

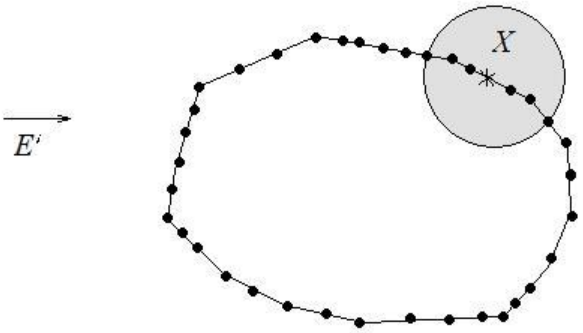

Figure 2. Nodes at the cylinder cross-section boundary.

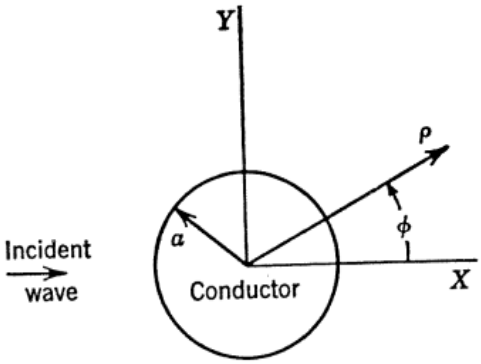

Figure 3. Problem geometry; circular cylinder cross-section

Taking the CFIE (30) for each observation point $\vec{x}_i$ and applying (31) to represent J_z in (30), we get the following linear system in $\boldsymbol{u}$:

$$\sum_{j=1}^{N} K_{ij}^{c}\,\hat{u}_j = f_i^c \tag{32}$$

where

$$K_{ij}^{c} = \alpha K_{ij}^{e} + (1-\alpha)\eta K_{ij}^{m} \tag{33}$$

$$f_i^{c} = \alpha f_i^{e} + (1-\alpha)\eta f_i^{m} \tag{34}$$

$$K_{ij}^{e} = \frac{\omega\mu}{4}\oint \phi_j(\vec{x}')H_0^{(2)}(kR)\,dl' \tag{35}$$

$$K_{ij}^{m} = \frac{1}{2}\phi_j(\vec{x}_i) + \frac{jk}{4}\oint \phi_j(\vec{x}')H_1^{(2)}(kR)\left[\hat{\boldsymbol{n}}\cdot\hat{R}\right]dl' \tag{36}$$

$$f_i^{e} = E_z^i(\vec{x}_i) \tag{37}$$

$$f_i^{m} = \left\{\hat{n}\times\vec{H}_i(\vec{x}_i)\right\}.\hat{z} \tag{38}$$

and $H_1^{(2)}$ is the first order Hankel function of the second type. In (36) and (38), the coefficients have been obtained from (29) after some vector manipulation. Once the $\hat{u}_i$ parameters are found, the surface current density at a given $\vec{x}$ can be determined by first finding the nodes that influence $\vec{x}$ and then applying (32). K^c is symmetrical, but it is not sparse. This shortcoming is due to the fact that the Hankel functions centered at a node extend over the whole domain, thus making any coefficient K_{ij}^{c} different from zero.

IV. NUMERICAL RESULTS

In order to evaluate the convergence of the solutions provided by the discretizations via MLS and IMLS shape functions, we have chosen the scattering of a plane wave by a circular perfect electric conductor (PEC) cylinder. This problem possesses analytical solution, thus providing means to study the precision of the numerical results. The scattering equations can be specialized for a circular cylinder through use of polar coordinates (ρ,φ) to locate a point at the cylinder surface.

As the radius of the cross section is constant ($\rho = a$), the equations become functions of φ alone. Fig. 3 illustrates the geometry of the problem.

At the cylinder surface $\rho = a$, the incident field is expressed as:

$$E_z^i(\vec{x}) = E_z^i(\vec{\rho}) = E_z^i(\rho,\varphi) = E_z^i(\varphi) = E_0 e^{-jka\,\cos\varphi} \tag{40}$$

In performing the plane-wave scattering analysis for a PEC cylinder with radius $a = 10\lambda$ and for an incoming plane wave having unit amplitude, the number of nodes uniformly distributed over the circular perimeter was gradually increased from 10 to 600. MLS approximation has had $\boldsymbol{p}^T = [1, x, y]$ as a linear basis and for the IMLS counterpart a three-term basis $\boldsymbol{p}^T = [p_1, p_2, p_3]$ has been used (built through the recursive expression (18) with $m = 3$).

It was found that when the number of nodes is greater than 100, the solution begins to converge, when compared to the analytical solution [7]:

$$J_z(\vec{\rho}) = \frac{2E_0}{\pi a\omega\mu}\sum_{n=-\infty}^{+\infty} j^{-n}\frac{e^{jn\varphi}}{H_n^{(2)}(ka)} \tag{41}$$

where φ is the observation angle along the circular contour and $H_n^{(2)}$ is the *n*-th order Hankel function of the second type.

To study the convergence of the results, the following RMS norm was used as a measure of the error between the numerical and analytical solutions:

$$norm = \sqrt{\frac{1}{2\pi a}\oint \left[J_{z_{Analytical}} - J_{z_{Numerical}}\right]^2 dl'} \tag{42}$$

Fig. 4 shows a log-log plot of the error norm as a function of the discretization length *h*, where *h* is the distance between two consecutive nodes along the circular contour. A linear regression applied to the rectilinear portion of the graph (abscissa greater than 0.8) shows that the convergence rates are approximately 2.36 for the MLS approximation and 1.36 for the IMLS, when the CFIE is employed. Besides that, the error inherent to the IMLS approximation is greater than that for the MLS.

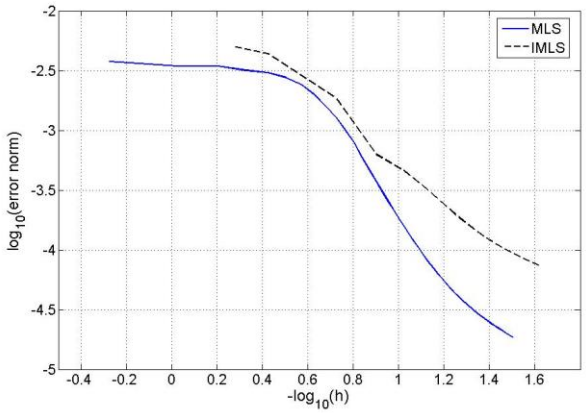

Figure 4. Convergence of the error norm as a function of the discretization length h for both approximations, MLS and IMLS.

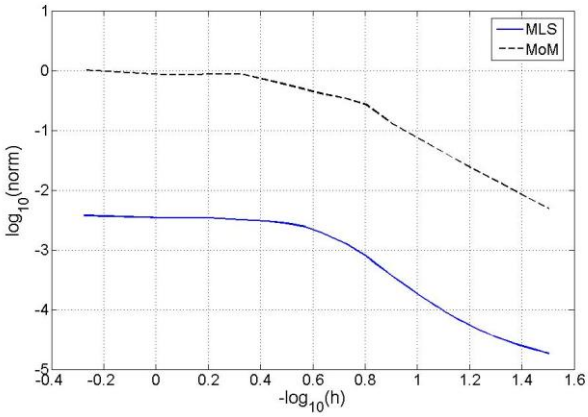

Figure 5. Convergence of the error norm as a function of the discretization length h for MoM (unit pulse basis and delta testing functions) and the MLS approximation.

The results seem to indicate that the scenario for IMLS is worse; its convergence rate is smaller and its error is greater. But on the other hand, the MLS approximation does not always work; for some scatterer geometries, the $\boldsymbol{A}$ matrix becomes singular, thus preventing the determination of the shape functions (e. g. for a cylinder with rectangular cross-section). This does not occur for the IMLS approximation, because its associated matrix $\overline{\boldsymbol{A}}$ does not need to be inverted.

A shortcoming common to both approximations is that the impedance matrix K^c given by (32) is not sparse (although symmetric). This is due to the integral formulation employed; the Hankel functions (playing the role of Green's functions) extend over the whole domain. Another common integral formulation is that of MoM, which discretizes the field equations through unit pulse basis and Dirac delta testing functions (point matching). Fig. 5 compares the error norm for MoM and the MLS approximation. A linear regression applied to the portion of the graph where the inclination is steepest (abscissa between 0.8 and 1.1) shows that the convergence rates are approximately 3.07 for the MLS and 2.66 for MoM.

V. CONCLUSIONS

In this work we have analyzed the plane-wave scattering by a PEC circular cylinder using the integral equations discretized by shape functions that occur in meshless methods. Among the various schemes for building the shape functions, we chose two of them: the MLS and the IMLS approximations. A comparison demonstrated that the MLS provides better results and converges faster than the IMLS, although the MLS approximation does not work for every geometry. The impedance matrix obtained from both approximations is fully populated, as would be expected from an integral formulation.

But one must bear in mind that what was done here was just a kind of experimentation, to verify how the shape functions would behave when employed in a problem that is traditionally solved through MoM. Meshless methods are suitable for differential formulations, and they are a substitute for FEM; the shape functions of the first are the counterpart of the triangular simplex ones used in the latter. But even when these shape functions have been applied in an integral formulation, the results are better than those provided by MoM (with unit basis and delta testing functions).

REFERENCES

[1] A. Peterson, S. Ray, and R. Mittra, *Computational Methods for Electromagnetics*, IEEE Press, 1998.

[2] G. Parreira, E. Silva, A. Fonseca, and R. Mesquita, "The Element-free Galerkin Method in 3-Dimensional Electromagnetic Problems", *IEEE Transactions on Magnetics*, vol. 42, no. 4, pp. 711-714, 2006.

[3] O. Bottauscio, M. Chiampi, and A. Manzin, "Element-free Galerkin method in eddy-current problems with ferromagnetic media", *IEEE Transactions on Magnetics*, vol. 42, no 5, pp. 1577-1584, 2006.

[4] A. Manzin, and O. Bottauscio, "Element-free galerkin method for the analysis of electromagnetic-wave scattering", *IEEE Transactions on Magnetics*, vol. 44, no 6, pp. 1366-1369, 2008.

[5] G. Liu, Mesh Free Methods: Moving Beyond the Finite Element Method, CRC Press, 2002.

[6] Peng M, Cheng Y. "A boundary element-free method (BEFM) for two-dimensional potential problems". *Engineering Analysis with Boundary Elements*, vol. 33, n°1, pp. 77-82, 2009

[7] C. Balanis, *Advanced Engineering Electromagnetics*, John Wiley & Sons, 1989.